

Article

Comparison of *Candida Albicans* Fatty Acid Amide Hydrolase Structure with Homologous Amidase Signature Family Enzymes

Cho-Ah Min ^{1,†}, Ji-Sook Yun ^{1,†}, Eun Hwa Choi ², Ui Wook Hwang ^{1,2}, Dong-Hyung Cho ³, Je-Hyun Yoon ⁴ and Jeong Ho Chang ^{1,2,*}

¹ Department of Biology Education, Kyungpook National University, Daegu 41566, Korea

² Research Institute for Phylogenomics and Evolution, Kyungpook National University, Daegu 41566, Korea

³ School of Life Sciences, Kyungpook National University, Daegu 41566, Korea

⁴ Department of Biochemistry and Molecular Biology, Medical University of South Carolina, Charleston, SC 29425, USA

* Correspondence: jhcbio@knu.ac.kr; Tel.: +82-53-950-5913

† These authors contributed equally to this work.

Received: 23 August 2019; Accepted: 8 September 2019; Published: 10 September 2019



Abstract: Fatty acid amide hydrolase (FAAH) is a well-characterized member of the amidase signature (AS) family of serine hydrolases. The membrane-bound FAAH protein is responsible for the catabolism of neuromodulatory fatty acid amides, including anandamide and oleamide, that regulate a wide range of mammalian behaviors, including pain perception, inflammation, sleep, and cognitive/emotional state. To date, limited crystal structures of FAAH and non-mammalian AS family proteins have been determined and used for structure-based inhibitor design. In order to provide broader structural information, the crystal structure of FAAH from the pathogenic fungus *Candida albicans* was determined at a resolution of 2.2 Å. A structural comparison with a brown rat *Rattus norvegicus* FAAH as well as with other bacterial AS family members, MAE2 and PAM, showed overall similarities but there were several discriminative regions found: the transmembrane domain and the hydrophobic cap of the brown rat FAAH were completely absent in the fungal FAAH structure. Along with these results, a phylogenetic analysis of 19 species within the AS family showed that fungal FAAHs diverged from a common ancestor before the separation of eukarya and prokarya. Taken together, this study provides insights into developing more potent inhibitors of FAAH as well as expanding our knowledge of the relationships between AS family members.

Keywords: fatty acid amide hydrolase; AS family; FAAH inhibitor; MAE2; PAM

1. Introduction

Fatty acid amide hydrolase (FAAH) is a well-characterized member of the amidase signature (AS) family containing a highly conserved sequence called the amidase consensus sequence, which is rich in serine and glycine residues [1]. There are five members of the AS family as peptide amidase (PAM), malonamidase E2 (MAE2), subunit A of Glu-tRNA^{Gln} amidotransferase, 6-aminohexanoate-cyclic-dimer hydrolase, and FAAH [2–6]. Members of the AS family include more than 200 proteins from over 90 different organisms from bacteria to humans and are involved in a variety of important biological functions. This family of enzymes is evolutionarily distinct but has diverged to develop a wide range of substrate specificities.

FAAH is a membrane-bound enzyme expressed in the brain, small intestine, pancreas, and muscle (skeletal and cardiac) that is responsible for the catabolism of neuro-modulatory fatty acid amide molecules including anandamide (AEA) and oleamide [7]. These signaling molecules regulate a

wide range of mammalian behaviors including appetite, motility, sleep, and cognitive/emotional state, in addition to being involved in pain perception and inflammatory responses. Catabolism of AEA by FAAH results in the production of ethanolamine and arachidonic acid (AA) [8]. The endogenous cannabinoid (i.e.; endocannabinoid) system is comprised of two cannabinoid receptors (CB1 and CB2) and the endocannabinoids, AEA and 2-arachidonylglycerol (2-AG) [9]. Other compounds have been shown to bind to CB1 and CB2 but these may have limited effects in organisms.

There is currently a great deal of interest in developing FAAH inhibitors to disrupt endocannabinoid signaling [10,11]. Since FAAH was identified as a drug target, numerous potent and selective FAAH inhibitors (e.g., URB, PF, OL, BIA, macamides, etc.) have been synthesized and reported [12–19]. Inhibiting the degradation of endogenous signaling molecules provides an attractive approach for therapeutic intervention since this approach may prevent side effects related to direct cannabinoid receptor agonism by synthetic molecules [20]. Because FAAH blockade only potentiates an activated signaling pathway by raising the endogenous concentration of the lipid-signaling molecule at its site of action, this blockade provides a temporal and spatial pharmacological control that is not typically available to a more classic agonist directly acting to a receptor. Mice completely lacking FAAH sense less pain and have less motility [21].

Only a few crystal structures are currently available for AS family members. These include the structures of FAAH from *Rattus norvegicus*, malonamidase E2 (MAE2) from *Bradyrhizobium japonicum*, peptide amidase (Pam) from *Stenotrophomonas maltophilia*, glutamyl-tRNA^{Gln} amidotransferases from *Staphylococcus aureus*, and a 6-aminohexanoate cyclic dimer hydrolase from *Arthrobacter* sp. [2–6]. Structural studies of the FAAH protein elucidate the action mechanism of the inhibitor using a series of inhibitors and FAAH from *Rattus norvegicus* (RnFAAH). However, no other structural reports, such as comparisons with other orthologous structures have been reported. Moreover, the functional variety and the wide evolutionary distribution of AS family enzymes underscore the importance of determining the three-dimensional structure of these enzymes in order to understand the structure–function relationship.

In order to provide a broader view of the three-dimensional structure and to suggest a structural basis for the widely varying individual substrate specificities of AS family enzymes, we determined the crystal structure of FAAH from the pathogenic fungus *Candida albicans* at a resolution of 2.2 Å. Based on structural analysis of *Candida albicans* FAAH (CaFAAH), we compared the newly determined structure with that of RnFAAH as well as those of the *Bradyrhizobium japonicum* MAE2 and *Stenotrophomonas maltophilia* peptide amidase (Pam). Furthermore, using both structure and sequence comparisons, the evolutionary relationship between AS family members was investigated based on their phylogenetic relationships. Ultimately, this study may provide insight into the development of more potent or widely used inhibitors for FAAH.

2. Materials and Methods

2.1. Cloning of FAAH from *Candida Albicans*

The CaFAAH gene was amplified from a *Candida albicans* genomic DNA library using the polymerase chain reaction (PCR), as described in a previous study [22]. Briefly, the amplified fragment was digested with the restriction enzymes NheI and XhoI (R016S and R0075, respectively, Enzymomics, Daejeon, Republic of Korea), and was ligated into pET26b vectors using T4 DNA ligase (M0202S, Roche, Basel, Switzerland). The plasmid was then transformed into *Escherichia coli* (*E. coli*) strain DH5 α , and the transformants were confirmed using colony PCR. All oligonucleotides used in the study were purchased from Cosmogenetech (Seoul, Republic of Korea).

2.2. Purification of Recombinant Proteins

The plasmid encoding CaFAAH was transformed into *E. coli* strain BL21 (DE3). Cells were grown and induced with 0.3 mM isopropyl β -D-1-thiogalactopyranoside (IPTG; 420322, Calbiochem,

Sigma-Aldrich, St. Louis, MO, USA) for 16 hr at 20 °C in LB medium (L4488, MCell, Seoul, Republic of Korea). The harvested cells were disrupted by ultra-sonication. The lysate was bound to Ni-NTA agarose (30230, Qiagen, Hilden, Germany) for 90 min at 4 °C. After washing with buffer A (200 mM NaCl, 50 mM Tris, pH 8.0) containing 20 mM imidazole (I5513, Sigma-Aldrich, USA), the bound proteins were eluted with 250 mM imidazole in buffer A. Size-exclusion chromatography (SEC) was performed using HiPrep 16/60 Sephacryl S-300 HR (17116701, GE Healthcare, Chicago, IL, USA). The buffer used for SEC contained 150 mM NaCl, 2 mM dithiothreitol (DTT; 233155, Calbiochem, Sigma-Aldrich, St. Louis, MO, USA), and 20 mM Tris, pH 7.5. Following SEC, the protein was stored at −80 °C pending crystallization trials.

To overcome the phasing problem, we produced a selenomethionine-substituted protein. Plasmids encoding *CaFAAH* were transformed into the methionine auxotrophic *E. coli* strain B834 (DE3) and cultured using a synthetic M9 minimal medium [23]. Cells were grown and induced with the same procedure as in the LB medium. His-tag affinity chromatography using Ni-NTA agarose and SEC was performed using the same method as the native *CaFAAH* purification process. To preserve the oxidation of the Se-Met crystals, the buffer used contained 150 mM NaCl, 10 mM dithiothreitol (DTT; 233155, Calbiochem, USA), and 25 mM Tris/HCl at pH 7.5 (Sigma-Aldrich, USA).

2.3. Crystallization

All crystallization trials were performed at 7 °C using either sitting-drop or hanging-drop vapor diffusion methods. *CaFAAH* crystals grew within a day in the crystallization condition of 30% *w/v* polyethylene glycol (PEG) 4000, 200 mM lithium sulfate, and 100 mM Tris/HCl, pH 8.5. The selenomethionine-derivatized *CaFAAH* crystals were tested under similar conditions to that of the native crystals of *CaFAAH* but conditions included the presence of 10 mM DTT. Prior to flash cooling all crystals in liquid nitrogen, 20% glycerol was added to the reservoir solution as a cryoprotectant.

2.4. Data Collection and Structure Determination

All diffraction datasets were collected at 100 K on the beamline 7A at the Pohang Accelerator Laboratory (PAL; Pohang, Republic of Korea) using a Quantum 270 CCD detector (San Jose, CA, USA). Data were processed using the *HKL-2000* suite [24]. Crystals of the selenomethionine-derivatized *CaFAAH* belonged to space group $P2_1$ and they diffracted to a resolution of 2.2 Å. The crystal structures were solved with single-wavelength anomalous diffraction phasing methods using the *PHENIX.autoSol* program in the PHENIX package version 1.9-1692 [25]. Model building was performed using the Wincoot program [26]. The structural models were refined using the *PHENIX.refine* program. Data collection details and statistics are provided in Table 1.

Table 1. Data collection and refinement statistics for *Candida albicans* fatty acid amide hydrolase.

Crystallographic Data	<i>CaFAAH</i>
Data collection	
Space group	$P2_1$
Cell dimensions	
a, b, c (Å)	84.8, 68.7, 100.9
α , β , γ (°)	90, 99.6, 90
Resolution range (Å)	50.0–2.28 (2.28–2.20) ^a
R_{merge} (%) ^b	10.4 (64.6)
$I / \sigma I$	13.03 (4.66)
Completeness (%)	99.8 (98.5)
Redundancy	7.0 (7.4)

Table 1. Cont.

Crystallographic Data	CaFAAH
Refinement	
Resolution	50.0–2.28
No. of reflections	58833
$R_{\text{work}}^c / R_{\text{free}}^d$ (%)	17.27 / 21.97
No. of atoms	9560
Protein	8962
Water	598
B-factors	
Protein	33.40
R.M.S. deviation	
Bond lengths (Å)	0.009
Bond angles (°)	1.21
PDB code	6KVR

^a The numbers in parentheses are statistics from the highest resolution shell; ^b $R_{\text{merge}} = \sum |I_{\text{obs}} - I_{\text{avg}}| / I_{\text{obs}}$, where I_{obs} is the observed intensity of individual reflections and I_{avg} is averaged over symmetry equivalents; ^c $R_{\text{work}} = \sum ||F_{\text{o}}| - |F_{\text{c}}|| / \sum |F_{\text{o}}|$, where $|F_{\text{o}}|$ and $|F_{\text{c}}|$ are the observed and calculated structure factor amplitudes, respectively; ^d R_{free} was calculated using 5% of the data.

2.5. Phylogenetic Analysis

The amino acid sequences of CaFAAH and other relevant species were obtained from the National Center for Biotechnology Information (NCBI) database (Table 2). Amino acid sequences were aligned using *ClustalW* [27]. Only well-aligned and conserved alignment sites were extracted from each alignment subset using *Gblock* (v0.91b) [28]. The phylogenetic tree was reconstructed with the maximum likelihood method using the *PhyML* program (v3.1/3.0) [29]. aLRT graphical representation of the phylogenetic tree (cladogram) was produced using *TreeDyn* from the *PHYMLIP package* (v3.66), which is available at the website (<http://www.phylogeny.fr/>).

Table 2. Sequence information for the consensus cladogram.

Protein	Species	NCBI Reference Sequence
FAAH (Fatty acid amide hydrolase)	<i>Danio rerio</i>	NP_001103295.1
	<i>Homo sapiens</i>	NP_001432.2
	<i>Xenopus laevis</i>	OCT82705.1
	<i>Bos Taurus</i>	DAA31035.1
	<i>Rattus norvegicus</i>	NP_077046.1
Glutamyl-tRNA (Gln) Amidotransferase	<i>Helicobacter pylori</i>	WP_000631451.1
	<i>Listeria monocytogenes</i>	WP_061104924.1
Malonamidase	<i>Bradyrhizobium Japonicum</i>	WP_011087863.1
Peptide Amidase	<i>Stenotrophomonas maltophilia</i>	CAC93616.1
Amidase	<i>Rhizobiales bacterium</i>	WP_037017835.1
	<i>Pseudomonas geniculate</i>	WP_057502485.1
	<i>Haloterrigena jeotgali</i>	WP_049965501.1
	<i>Methylobacterium radiotolerans</i>	WP_012319231.1
	<i>Saccharomyces cerevisiae</i> *	CAA39514.1
	<i>Penicillium italicum</i>	KGO69811
	<i>Debaryomyces hansenii</i> *	XP_457833.2
	<i>Kluyveromyces lactis</i> *	XP_451920.1
	<i>Candida albicans</i> *	XP_716991.1
<i>Schizosaccharomyces pombe</i> *	NP_588099.1	

* Indicates putative protein.

3. Results

3.1. Overall Structure of CaFAAH

Two molecules of CaFAAH were found in the asymmetric unit and each monomer in the dimeric CaFAAH was positioned with two-fold symmetry (Figure 1A). There are two functional regions in the dimeric structure. In the first region, both the α 13- β 7 and β 5- β 6 loops are mainly involved in dimerization through interactions with α 18 helices in their partner molecules (Figure 1A). In the second functional region, each of the α 1- α 2 loops is located on the same side of the dimer at a 90° rotation along the X-axis. As was also observed in the RnFAAH structure [4], this parallel orientation of each monomer has a role in substrate recruitment from the same side of the membrane.

The overall structure of the CaFAAH monomer consists of 11 central twisted β -sheets surrounded by 22 α -helices (Figure 1B). This structural arrangement is also present in previously reported FAAH structures from different species [14]. Furthermore, the structural fold could be presented as a feature of a broad range of AS family proteins. In the vicinity of the α 3, α 11, and β 4 helices, the central deep pocket contains a unique Ser-Ser-Lys triad, which plays an important role in the enzyme's hydrolase activity (Figure 1B,C). In addition, similar to other FAAHs, the pocket, also referred to as the active site, is located in the amidase signature domain. The oligomerization domain, which is involved in dimerization of the CaFAAH dimer and comprised of helix α 13 and part of loop α 1- α 2, is located outside of the central region (Figure 1B,C).

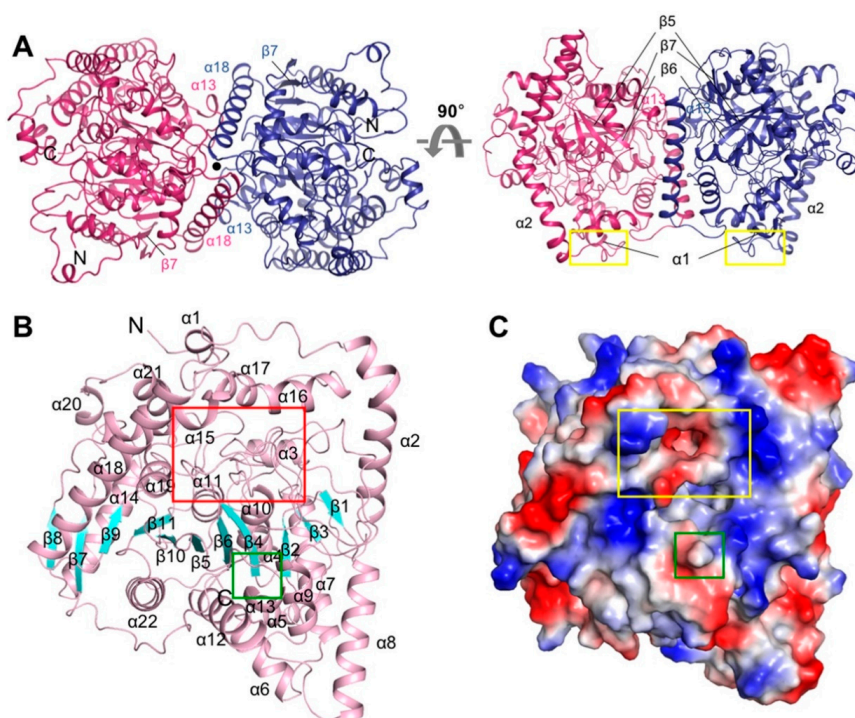


Figure 1. Overall structure of CaFAAH. (A) The dimeric structure of CaFAAH is shown in a ribbon diagram. The central two-fold axis of symmetry is indicated by a black circle. The right panel shows a 90° rotation along the X axis from the orientation of the left panel. The α 1- α 2 loops are highlighted in yellow boxes. (B) The monomeric structure of the CaFAAH 22-stranded α -helix is highlighted in a light-pink color and the 11-stranded β -sheet is highlighted in a light-blue color. The active site of CaFAAH is highlighted with a red box, and the oligomerization domain is highlighted with a green box. (C) The electrostatic surface presentation of the monomeric CaFAAH is shown with the same orientation as in Figure 1C. Each of the active sites and oligomerization domains are highlighted with a yellow and a green box, respectively.

3.2. Active Site

The catalytic triad signature comprised of residues Ser233, Ser257, and Lys158 is a main component of the active site in the *Ca*FAAH structure (Figure 2A). These residues are referred to as the AS sequence and are highly conserved among the amidase family members [30]. The Ser257 residue acts as the primary nucleophile that attacks the substrate and the Lys158 plays a role as a general acid/base (Figure 2B). Ser217 serves as a proton-shuttle between Lys158 and Ser257. In addition, four residues, namely Lys210, Ile254, Asn397, and Asn422 are expected to interact with the substrate and therefore are critical for the amidase activity of FAAH.

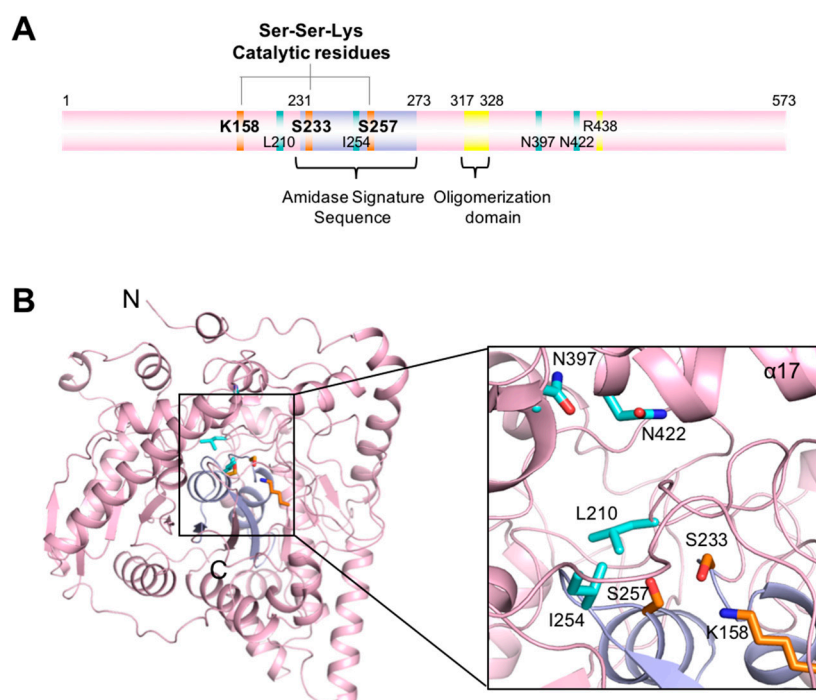


Figure 2. Domain organization and active site of *Ca*FAAH. (A) Schematic representation of the domain organization of *Ca*FAAH. The amidase signature domain is highlighted with a light-blue color and the oligomerization domain is highlighted in yellow. (B) Schematic of the overall structure including the active site highlighted with a black square in the left panel. The catalytic Ser-Ser-Lys triad (Ser257-Ser233-Lys158) is shown in orange, and the remainder of the active site residues (Leu210, Ile254, Asn397, and Asn422) are colored in light blue. A detailed view of the active site is shown in the right panel.

3.3. Comparison of *Ca*FAAH Structure with the AS Family Protein *Rn*FAAH

To assess the structural relationship between *Ca*FAAH and other AS family proteins, we searched for homologous structures using the DaLi server [31]. The output suggested that the structure with the greatest homology to *Ca*FAAH is FAAH from *Rattus norvegicus* (*Rn*FAAH; PDB code, 1MT5) with a Z-score of 45.5 and a root mean square deviation (r.m.s.d) value of 2.0 Å. A structure-based sequence comparison of *Ca*FAAH with *Rn*FAAH showed they were 26.74% identical with a high degree of conservation being especially noted for the AS sequence. However, there are several interesting differences in both the secondary structures and sequences (Supplementary Materials Figure S1).

While the overall structures of both *Ca*FAAH and *Rn*FAAH are similar, there are five discriminative regions in the overlaid structures. First, the α 20 helix in *Ca*FAAH, covering residues 511–518, is positioned \sim 8.8 Å outward compared to that of the equivalent helix in *Rn*FAAH (Figure 3A; box I). Second, a major difference is that the hydrophobic cap, composed of two helices (α 18 and α 19) connected by a hairpin loop covering residues 404–433 in *Rn*FAAH, is absent in the *Ca*FAAH structure (Figure 3A; box II). The proposed role of the hydrophobic cap in *Rn*FAAH is to assist in membrane

insertion of the N-terminal region [4]. Third, the secondary structure covering residues 330~335 in *CaFAAH* shows an $\alpha 13$ - $\beta 2$ loop but the equivalent region in *RnFAAH* forms an α -helix ($\alpha 11$) instead of a loop (Figure 3B; box III). Fourth, the oligomerization domain $\alpha 13$ helix covering residues 317~330 in *CaFAAH* has a different amino acid sequence but the same secondary structure as the $\alpha 10$ helix in the *RnFAAH* structure (Figure 3B; box IV, Supplementary Materials Figure S1). Therefore, the mode of dimerization should be similar in both structures. Finally, the N-terminal region covering residues 1~29 of *RnFAAH* is predicted to be a monotopic transmembrane domain. Therefore, the N-terminal part was excluded from the reported structure in order to improve the purification and crystallization of the protein [4]. However, the amino acid sequence of the equivalent region in *CaFAAH* is very different. Furthermore, since the full-length *CaFAAH* was crystallized, the structure of *CaFAAH* contains an N-terminal region comprising 25 amino acid residues that form two α -helices; these are not present in the *RnFAAH* structure (Figure 3B; box V, Supplementary Materials Figure S1).

Taken together, *CaFAAH* has several distinct structural features compared to *RnFAAH*. Of importance, two major hydrophobic patches that form the N-terminal transmembrane domain and the hydrophobic cap, respectively, are not present in the *CaFAAH* structure. These features suggest that *CaFAAH* has unique functions or may indicate evolutionary changes reflective of fungal FAAHs within the broader AS family.

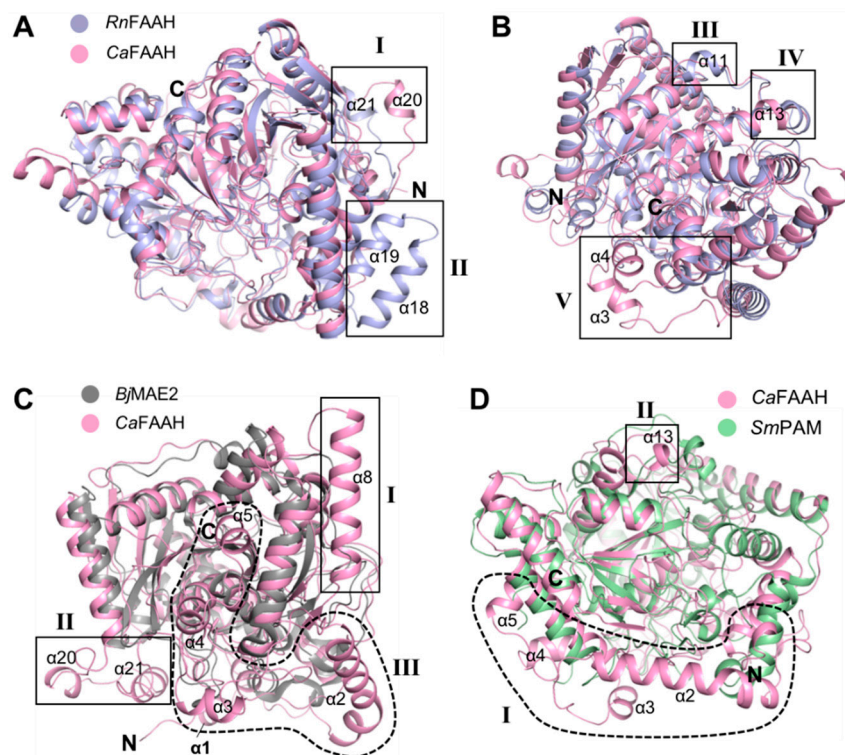


Figure 3. Structural comparisons of *CaFAAH* with AS family proteins. (A) The overall structures of *CaFAAH* and FAAH from *Rattus norvegicus* (*RnFAAH*) are depicted in light pink and light blue colors, respectively. The two different structural regions (I, II) are indicated by black squares with annotations. (B) View of 90° rotation along the X-axis from the orientation shown in Figure 3A. The three discriminative structural elements (III, IV, V) are shown in black squares with their annotations. (C) The overall structures of *CaFAAH* and *BjMAE2* are depicted in light pink and gray colors, respectively. The three varied structural elements (I, II, III) are shown in black squares and dashed lines with their annotations. (D) The overall structures of *CaFAAH* and *SmPAM* are depicted in light-pink and green colors, respectively. The two mismatched structural elements (I, II) are shown in black squares and dashed lines with their annotations.

3.4. Comparison of CaFAAH Structure with AS Family Proteins BjMAE2 and SmFAM

Other than RnFAAH, two more crystal structures in the AS family have been reported, namely malonamidase (MAE2) from *Bradyrhizobium japonicum* (BjMAE2; PDB code, 1OCK) and peptide amidase (PAM) from *Stenotrophomonas maltophilia* (SmFAM; PDB code, 1M22) [3,32]. We also compared these two structures with that of CaFAAH using a pair-wise analysis of the DaLi server [31].

A comparison of the structure-based sequence alignment between CaFAAH and BjMAE2 showed the two proteins were 23.18% identical (Supplementary Materials Figure S2), with a Z-score of 40.4 and an r.m.s.d of 2.3 Å. However, there were three regions of difference in the overlaid structures (Figure 3C). First, the CaFAAH structure contained five additional α -helices ($\alpha 1$ – $\alpha 5$) in its N-terminus, as well as two α -helices ($\alpha 20$ – $\alpha 21$) near the C-terminus; no equivalent regions were found in BjMAE2 (Figure 3C; boxes I, II). In addition, the $\beta 1$ - $\beta 2$ loop covering 20 residues in BjMAE2 was substituted with an α -helix ($\alpha 8$) in the CaFAAH structure (Figure 3C; dashed region III).

A comparison of the structure-based sequence alignment between CaFAAH and SmPAM showed the two proteins were 24.74% identical (Supplementary Materials Figure S3), with a Z-score of 36.6 and an r.m.s.d. of 2.4 Å. These values indicated that the similarity of SmPAM to CaFAAH was somewhat lower than that of BjMAE2. There were also two regions of significant difference in the superposed structures (Figure 3D). First, similar to the overlaid CaFAAH and BjMAE2 structures, five N-terminal α -helices ($\alpha 1$ – $\alpha 5$) in CaFAAH were absent in the structure of SmPAM (Figure 3D; dashed region I) and second, the $\alpha 8$ - $\alpha 9$ loop of SmPAM was present as the $\alpha 13$ helix in the CaFAAH structure (Figure 3D; box II).

3.5. Comparison of CaFAAH Active Site with the RnFAAH-Inhibitor Complexes

Several crystal structures of RnFAAH in complexes with inhibitors have been reported, including N-phenyl-4-(quinolin-2-ylmethyl) piperidine-1-carboxamide (PF-750) [4,13], cyclohexyl carbamic acid 3' carbamoyl biphenyl-3-yl ester (URB597) [14], and methyl arachidonoyl fluorophosphonate (MAFP) [4]. Superimposing the structure of CaFAAH onto the three RnFAAH-inhibitor complexes revealed that most of the residues that interact with the inhibitors were overlaid (Fig. 4). Residues Ser233, Lys158, S257, and Ile254 in CaFAAH were especially well matched to those of the equivalent residues in RnFAAH (Ser217, Lys142, Ser241, and Ile238). Therefore, CaFAAH likely interacts with these three inhibitors (PF-750, URB597, and MAFP) in a similar fashion to RnFAAH.

A comparison of CaFAAH with the RnFAAH-PF-750 complex (PDB code: 2VYA) showed that Leu210, Met208, and His393 of CaFAAH may interact with the pyridine ring of PF-750 in addition to the residues of the catalytic triad (Figure 4A). However, Trp481 from CaFAAH, which is equivalent to Ile491 from RnFAAH, clashed with the PF-750 inhibitor, suggesting there may be a different conformation for PF-750 in CaFAAH. Furthermore, residues Phe432 and Thr488 in RnFAAH, which interact with the quinolone ring of PF-750, were not found in the structure of CaFAAH (Figure 4A). These observations suggest that the binding affinity of PF-750 for CaFAAH may be lower than that for RnFAAH.

A comparison of CaFAAH with the RnFAAH-URB597 complex (PDB code: 3LJ6) indicated that residues Met208 and Leu210 from CaFAAH may interact with the pyridine ring of URB597 (Figure 4B). However, His393 from CaFAAH (which has no equivalent residue in RnFAAH) was incompatible with URB597, and it is therefore presumed that the URB597 inhibitor may have an altered conformation at the active site of CaFAAH. Moreover, RnFAAH's residues Phe432 and Tyr488, which interact with the pyridine and phenol rings of URB597, do not exist in the CaFAAH structure (Figure 4B).

The comparison of CaFAAH with the RnFAAH-MAFP complex (PDB code: 1MT5) showed that the Met208 and Leu210 residues from CaFAAH may interact with the aliphatic chain of MAFP in a manner similar to URB597 (Figure 4C). However, in this model, both His393 and Trp481 in CaFAAH are also incompatible with MAFP, which is likely to affect MAFP localization in CaFAAH. As with the PF-750 and URB597 inhibitors, RnFAAH residues Phe432 and Thr488, which are responsible for forming an interaction with the aliphatic chain of MAFP, do not exist in CaFAAH (Figure 4C). Interestingly, MAFP contains a fluorophosphonate group where the position of the oxygen atom in the group is equivalent to that of the water molecule (W1) shown in the PF-750 and URB597 complex

structure (Figure 4). Therefore, the Ser233 residue from *Ca*FAAH may interact with the oxygen atom in the fluorophosphonate group of MAFP instead of a water molecule as was seen in the two other complexes (Figure 4C).

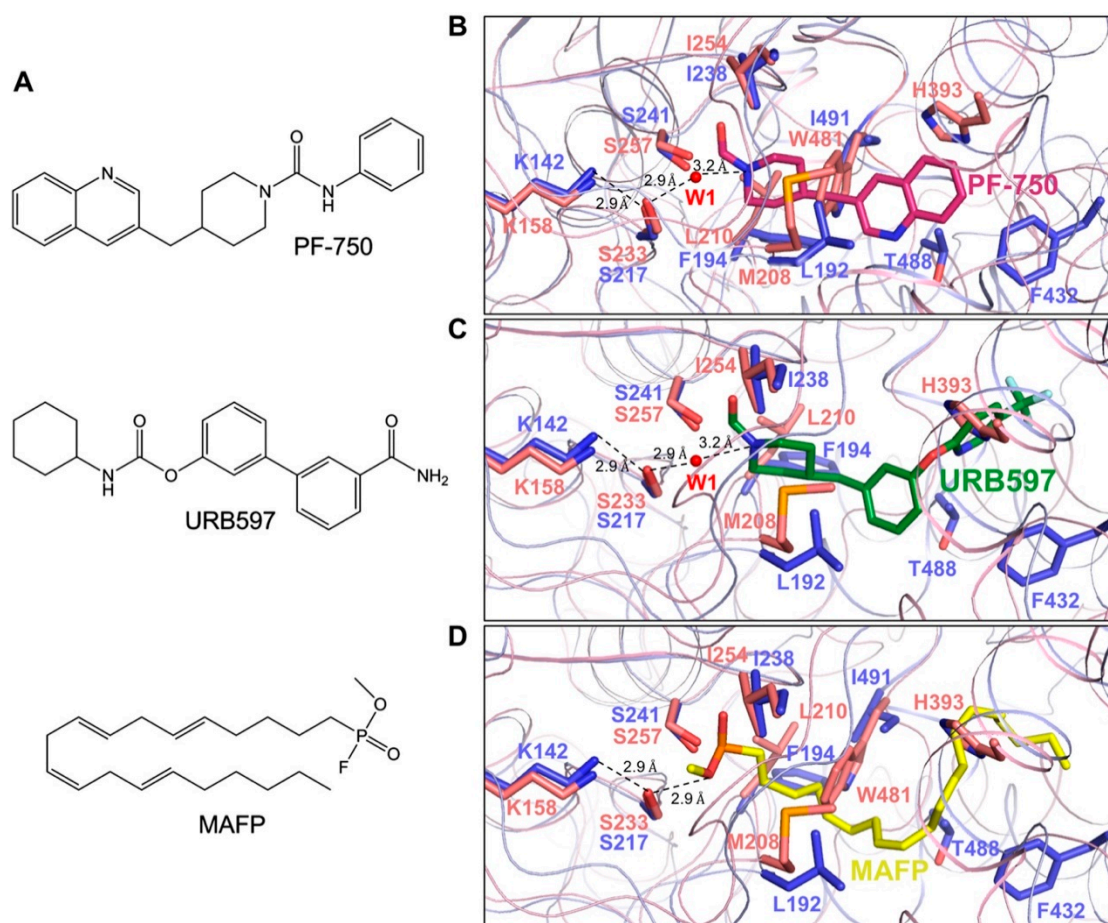


Figure 4. Superposition of the structures of *Ca*FAAH and *Rn*FAAH-inhibitor complexes. (A) A detailed view of the interaction between PF-750 and overlaid *Ca*FAAH with *Rn*FAAH (PDB code, 2VYA). Residues from *Ca*FAAH and *Rn*FAAH are shown in salmon and deep blue colors, respectively. The inhibitor PF-750 is shown in a deep pink color. The water molecule W1 is shown as a red sphere. (B) A detailed view of the interaction between URB597 and overlaid *Ca*FAAH with *Rn*FAAH (PDB code, 3LJ6). Residues from *Ca*FAAH and *Rn*FAAH are shown in salmon and deep blue colors, respectively. The inhibitor URB597 is shown in green. The water molecule W1 is represented by a red sphere. (C) A detailed view of the interaction between MAFP and overlaid *Ca*FAAH with *Rn*FAAH (PDB code, 1MT5). Residues from *Ca*FAAH and *Rn*FAAH are shown in salmon and deep-blue colors, respectively. The inhibitor MAFP is shown in yellow.

3.6. Phylogenetic Analysis of AS Family Proteins

Based on the local structural differences found, we investigated the phylogenetic relationships and evolutionary distances among 19 members of the AS family (Table 2). *Ca*FAAH is phylogenetically closely related to both *Kluyveromyces lactis* FAAH and *Debaryomyces hansenii* FAAH, indicating that fungal FAAH could be categorized to a monophyletic taxon (Figure 5). Likewise, bacteria, fungi, and higher eukaryotes converge to a polyphyletic taxon. This result indicates that AS-containing genes already existed in common ancestors prior to the divergence of prokarya and eukarya [33]. In addition, for the three AS family members that we previously compared using structural analysis, *Ca*FAAH is more closely related to *Rn*FAAH than either *Bj*MAE2 or *Sm*PAM based on the phylogenetic analysis.

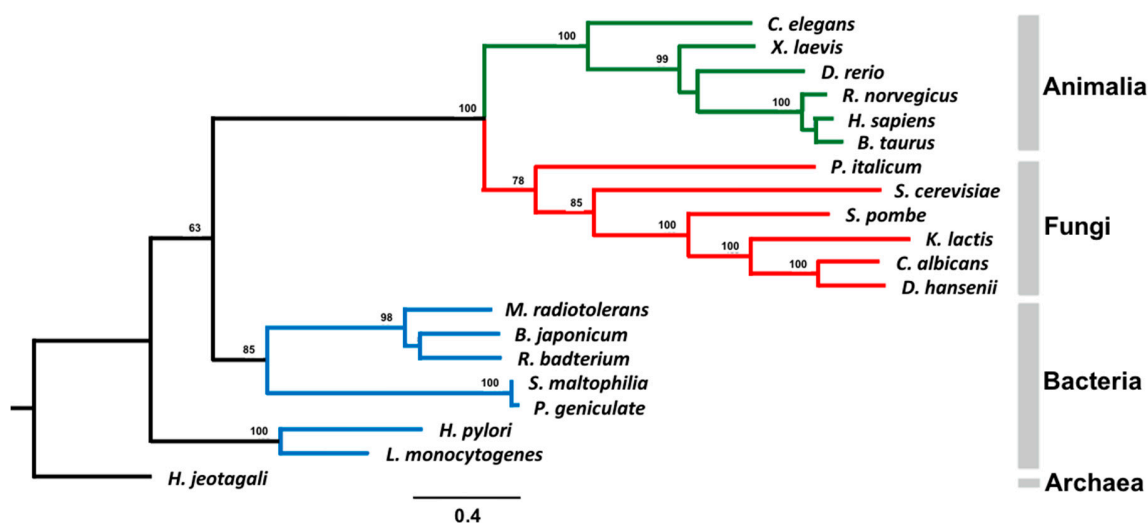


Figure 5. Phylogenetic tree of AS family proteins. Alignment of protein sequences was carried out using *ClustalW* [27] and the phylogenetic tree was produced using the *PHYLIP* package program.

4. Discussion

The AS family of proteins, which contains the amidase consensus sequence, plays important roles in biological processes. They are bifunctional enzymes with both intrinsic amidase and esterase/peptidase activities, able to cleave ester, amide, and nitrile bonds depending on their enzyme-specific ratios [34–37]. Currently, a large number of proteins containing AS sequences has been identified, including amidases and aspartic proteinases that may form part of this family [38]. Among them, FAAH, MAE2, PAM, subunit A of Glu-tRNA^{Gln} amidotransferase, and 6-aminohexanoate cyclic dimer hydrolase are considered representative members of the AS family that share somewhat conserved active sites [38].

Among the five members of the AS family, FAAH, which contains a common catalytic triad (Ser-Ser-Lys), is characterized as being able to hydrolyze amide bonds [1]. Moreover, because FAAH is highly involved in the neuronal signal transduction pathways that relay pain, many groups have focused on developing potent chemical inhibitors using *Rn*FAAH [10]. Therefore, there have been several reports on the crystal structures of *Rn*FAAH in complexes with inhibitors [16,39–43]. Because there is limited structural information about FAAHs beyond *Rn*FAAH, it is necessary to compare structures homologous with *Rn*FAAH to expand our knowledge of the functional aspects of FAAH. Such a comparison may also provide new information for drug development.

Comparisons with the structures of AS family members revealed several critical differences, such as the presence of an N-terminal non-hydrophobic helical region corresponding to the transmembrane domain of *Rn*FAAH (Supplementary Materials Figure S1). In addition, the hydrophobic cap in *Rn*FAAH was not present in the *Ca*FAAH, *Bj*MAE2, and *Sm*PAM structures. Furthermore, the N-terminal region of *Ca*FAAH was completely absent in *Bj*MAE2 and *Sm*PAM (Supplementary Materials Figures S2 and S3). These discrepancies in the structure/sequence may be indicative of the evolutionary developments/diversity of FAAH proteins. Our phylogenetic analysis showed that AS family members including FAAH proteins were clearly converged to a polyphyletic taxon from a common ancestor. Moreover, although limited structural reports are available, there may be an evolutionary correlation between the sequence and structure of AS family members.

Taken together, the structural information presented here and the phylogenetic analysis of *Ca*FAAH may provide insights into developing broader, more effective, potent drugs for the treatment of pain in addition to having implications in the divergence of enzymes. However, further studies with fungal FAAHs are required to uncover their physiological substrates as well as to understand their biological relationships with higher eukaryotic FAAH proteins.

Supplementary Materials: The following are available online at <http://www.mdpi.com/2073-4352/9/9/472/s1>.

Author Contributions: Cloning, protein purification, crystallization, C.-A.M.; Diffraction data collection and analysis, C.-A.M.; J.-S.Y.; J.H.C.; Phylogenetics, C.-A.M.; E.H.C.; U.W.H.; Enzymology, D.H.C.; Supervision, J.-H.Y.; J.H.C.; Writing—original draft, C.-A.M.; J.H.C.; Writing—review & editing, J.-H.Y., J.H.C.

Funding: This research was supported by Kyungpook National University Bokhyeon Research Fund, 2017 to J.H.C.; and Medical University of South Carolina Startup fund to J.-H.Y.

Acknowledgments: We would like to thank beamline staffs Yeon-Gil Kim and Sung Chul Ha at beamlines 5C and 7A of the Pohang Accelerator Laboratory (Pohang, Korea) for data collection.

Conflicts of Interest: The authors declare no conflicts of interest.

References

1. Patricelli, M.P.; Lovato, M.A.; Cravatt, B.F. Chemical and mutagenic investigations of fatty acid amide hydrolase: Evidence for a family of serine hydrolases with distinct catalytic properties. *Biochemistry* **1999**, *38*, 9804–9812. [[CrossRef](#)] [[PubMed](#)]
2. Labahn, J.; Neumann, S.; Buldt, G.; Kula, M.R.; Granzin, J. An alternative mechanism for amidase signature enzymes. *J. Mol. Biol.* **2002**, *322*, 1053–1064. [[CrossRef](#)]
3. Shin, S.; Lee, T.H.; Ha, N.C.; Koo, H.M.; Kim, S.Y.; Lee, H.S.; Kim, Y.S.; Oh, B.H. Structure of malonamidase E2 reveals a novel Ser-cisSer-Lys catalytic triad in a new serine hydrolase fold that is prevalent in nature. *EMBO J.* **2002**, *21*, 2509–2516. [[CrossRef](#)] [[PubMed](#)]
4. Bracey, M.H.; Hanson, M.A.; Masuda, K.R.; Stevens, R.C.; Cravatt, B.F. Structural adaptations in a membrane enzyme that terminates endocannabinoid signaling. *Science* **2002**, *298*, 1793–1796. [[CrossRef](#)] [[PubMed](#)]
5. Yasuhira, K.; Shibata, N.; Mongami, G.; Uedo, Y.; Atsumi, Y.; Kawashima, Y.; Hibino, A.; Tanaka, Y.; Lee, Y.H.; Kato, D.; et al. X-ray crystallographic analysis of the 6-aminohexanoate cyclic dimer hydrolase: Catalytic mechanism and evolution of an enzyme responsible for nylon-6 byproduct degradation. *J. Biol. Chem.* **2010**, *285*, 1239–1248. [[CrossRef](#)] [[PubMed](#)]
6. Nakamura, A.; Yao, M.; Chimnarok, S.; Sakai, N.; Tanaka, I. Ammonia channel couples glutaminase with transamidase reactions in GatCAB. *Science* **2006**, *312*, 1954–1958. [[CrossRef](#)]
7. Ahn, K.; McKinney, M.K.; Cravatt, B.F. Enzymatic pathways that regulate endocannabinoid signaling in the nervous system. *Chem. Rev.* **2008**, *108*, 1687–1707. [[CrossRef](#)]
8. Bradshaw, H.B.; Rimmerman, N.; Hu, S.S.; Benton, V.M.; Stuart, J.M.; Masuda, K.; Cravatt, B.F.; O'Dell, D.K.; Walker, J.M. The endocannabinoid anandamide is a precursor for the signaling lipid N-arachidonoyl glycine by two distinct pathways. *BMC Biochem.* **2009**, *10*, 14. [[CrossRef](#)]
9. Lu, H.C.; Mackie, K. An Introduction to the Endogenous Cannabinoid System. *Biol. Psychiatry* **2016**, *79*, 516–525. [[CrossRef](#)]
10. Ahn, K.; Johnson, D.S.; Mileni, M.; Beidler, D.; Long, J.Z.; McKinney, M.K.; Weerapana, E.; Sadagopan, N.; Liimatta, M.; Smith, S.E.; et al. Discovery and characterization of a highly selective FAAH inhibitor that reduces inflammatory pain. *Chem. Biol.* **2009**, *16*, 411–420. [[CrossRef](#)]
11. Ogawa, S.; Kunugi, H. Inhibitors of Fatty Acid Amide Hydrolase and Monoacylglycerol Lipase: New Targets for Future Antidepressants. *Curr. Neuropharm.* **2015**, *13*, 760–775. [[CrossRef](#)]
12. Deutsch, D.G.; Ueda, N.; Yamamoto, S. The fatty acid amide hydrolase (FAAH). *Prostaglandins Leukot. Essent. Fat. Acids* **2002**, *66*, 201–210. [[CrossRef](#)] [[PubMed](#)]
13. Mileni, M.; Johnson, D.S.; Wang, Z.; Everdeen, D.S.; Liimatta, M.; Pabst, B.; Bhattacharya, K.; Nugent, R.A.; Kamtekar, S.; Cravatt, B.F.; et al. Structure-guided inhibitor design for human FAAH by interspecies active site conversion. *Proc. Natl. Acad. Sci. USA* **2008**, *105*, 12820–12824. [[CrossRef](#)] [[PubMed](#)]
14. Mileni, M.; Kamtekar, S.; Wood, D.C.; Benson, T.E.; Cravatt, B.F.; Stevens, R.C. Crystal structure of fatty acid amide hydrolase bound to the carbamate inhibitor URB597: Discovery of a deacylating water molecule and insight into enzyme inactivation. *J. Mol. Biol.* **2010**, *400*, 743–754. [[CrossRef](#)] [[PubMed](#)]
15. Mileni, M.; Garfinkle, J.; Ezzili, C.; Cravatt, B.F.; Stevens, R.C.; Boger, D.L. Fluoride-mediated capture of a noncovalent bound state of a reversible covalent enzyme inhibitor: X-ray crystallographic analysis of an exceptionally potent alpha-ketoheterocycle inhibitor of fatty acid amide hydrolase. *J. Am. Chem. Soc.* **2011**, *133*, 4092–4100. [[CrossRef](#)] [[PubMed](#)]

16. Kono, M.; Matsumoto, T.; Kawamura, T.; Nishimura, A.; Kiyota, Y.; Oki, H.; Miyazaki, J.; Igaki, S.; Behnke, C.A.; Shimojo, M.; et al. Synthesis, SAR study, and biological evaluation of a series of piperazine ureas as fatty acid amide hydrolase (FAAH) inhibitors. *Bioorg. Med. Chem.* **2013**, *21*, 28–41. [[CrossRef](#)] [[PubMed](#)]
17. Bertolacci, L.; Romeo, E.; Veronesi, M.; Magotti, P.; Albani, C.; Dionisi, M.; Lambruschini, C.; Scarpelli, R.; Cavalli, A.; De Vivo, M.; et al. A binding site for nonsteroidal anti-inflammatory drugs in fatty acid amide hydrolase. *J. Am. Chem. Soc.* **2013**, *135*, 22–25. [[CrossRef](#)] [[PubMed](#)]
18. Huang, Z.; Ogasawara, D.; Seneviratne, U.I.; Cognetta, A.B., 3rd; Am Ende, C.W.; Nason, D.M.; Lapham, K.; Litchfield, J.; Johnson, D.S.; Cravatt, B.F. Global Portrait of Protein Targets of Metabolites of the Neurotoxic Compound BIA 10-2474. *ACS Chem. Biol.* **2019**, *14*, 192–197. [[CrossRef](#)]
19. Alasmari, M.; Bhlke, M.; Kelley, C.; Maher, T.; Pino-Figueroa, A. Inhibition of Fatty Acid Amide Hydrolase (FAAH) by Macamides. *Mol. Neurobiol.* **2019**, *56*, 1770–1781. [[CrossRef](#)]
20. Pacher, P.; Batkai, S.; Kunos, G. The endocannabinoid system as an emerging target of pharmacotherapy. *Pharmacol. Rev.* **2006**, *58*, 389–462. [[CrossRef](#)]
21. Cravatt, B.F.; Demarest, K.; Patricelli, M.P.; Bracey, M.H.; Giang, D.K.; Martin, B.R.; Lichtman, A.H. Supersensitivity to anandamide and enhanced endogenous cannabinoid signaling in mice lacking fatty acid amide hydrolase. *Proc. Natl. Acad. Sci. USA* **2001**, *98*, 9371–9376. [[CrossRef](#)] [[PubMed](#)]
22. Min, C.A.; Yun, J.S.; Yoon, J.H.; Chang, J.H. Purification, crystallization, and X-ray crystallographic analysis of fatty acid amide hydrolase from *Candida albicans*. *Biodesign* **2019**, *7*, 38–41. [[CrossRef](#)]
23. Ramakrishnan, V.; Finch, J.T.; Graziano, V.; Lee, P.L.; Sweet, R.M. Crystal structure of globular domain of histone H5 and its implications for nucleosome binding. *Nature* **1993**, *362*, 219–223. [[CrossRef](#)] [[PubMed](#)]
24. Otwinowski, Z.; Minor, W. Processing of X-ray diffraction data collected in oscillation mode. *Method Enzymol.* **1997**, *276*, 307–326.
25. Adams, P.D.; Afonine, P.V.; Bunkoczi, G.; Chen, V.B.; Davis, I.W.; Echols, N.; Headd, J.J.; Hung, L.W.; Kapral, G.J.; Grosse-Kunstleve, R.W.; et al. PHENIX: A comprehensive Python-based system for macromolecular structure solution. *Acta Crystallogr. Sect. D Biol. Crystallogr.* **2010**, *66*, 213–221. [[CrossRef](#)]
26. Emsley, P.; Cowtan, K. Coot: Model-building tools for molecular graphics. *Acta Crystallogr. Sect. D Biol. Crystallogr.* **2004**, *60*, 2126–2132. [[CrossRef](#)]
27. Thompson, J.D.; Higgins, D.G.; Gibson, T.J. CLUSTAL W: Improving the sensitivity of progressive multiple sequence alignment through sequence weighting, position-specific gap penalties and weight matrix choice. *Nucleic Acids Res.* **1994**, *22*, 4673–4680. [[CrossRef](#)]
28. Castresana, J. Selection of conserved blocks from multiple alignments for their use in phylogenetic analysis. *Mol. Biol. Evolut.* **2000**, *17*, 540–552. [[CrossRef](#)]
29. Guindon, S.; Gascuel, O. A simple, fast, and accurate algorithm to estimate large phylogenies by maximum likelihood. *Syst. Biol.* **2003**, *52*, 696–704. [[CrossRef](#)]
30. Cravatt, B.F.; Giang, D.K.; Mayfield, S.P.; Boger, D.L.; Lerner, R.A.; Gilula, N.B. Molecular characterization of an enzyme that degrades neuromodulatory fatty-acid amides. *Nature* **1996**, *384*, 83–87. [[CrossRef](#)]
31. Holm, L.; Rosenstrom, P. Dali server: Conservation mapping in 3D. *Nucleic Acids Res.* **2010**, *38*, W545–W549. [[CrossRef](#)] [[PubMed](#)]
32. Valina, A.L.; Mazumder-Shivakumar, D.; Bruice, T.C. Probing the Ser-Ser-Lys catalytic triad mechanism of peptide amidase: Computational studies of the ground state, transition state, and intermediate. *Biochemistry* **2004**, *43*, 15657–15672. [[CrossRef](#)] [[PubMed](#)]
33. Chebrou, H.; Bigey, F.; Arnaud, A.; Galzy, P. Study of the amidase signature group. *Biochim. Biophys. Acta* **1996**, *1298*, 285–293. [[CrossRef](#)]
34. Cilia, E.; Fabbri, A.; Uriani, M.; Scialdone, G.G.; Ammendola, S. The signature amidase from *Sulfolobus solfataricus* belongs to the CX3C subgroup of enzymes cleaving both amides and nitriles. Ser195 and Cys145 are predicted to be the active site nucleophiles. *FEBS J.* **2005**, *272*, 4716–4724. [[CrossRef](#)] [[PubMed](#)]
35. Shin, S.; Yun, Y.S.; Koo, H.M.; Kim, Y.S.; Choi, K.Y.; Oh, B.H. Characterization of a novel Ser-cisSer-Lys catalytic triad in comparison with the classical Ser-His-Asp triad. *J. Biol. Chem.* **2003**, *278*, 24937–24943. [[CrossRef](#)]
36. Patricelli, M.P.; Cravatt, B.F. Clarifying the catalytic roles of conserved residues in the amidase signature family. *J. Biol. Chem.* **2000**, *275*, 19177–19184. [[CrossRef](#)] [[PubMed](#)]

37. Gopalakrishna, K.N.; Stewart, B.H.; Kneen, M.M.; Andricopulo, A.D.; Kenyon, G.L.; McLeish, M.J. Mandelamide hydrolase from *Pseudomonas putida*: Characterization of a new member of the amidase signature family. *Biochemistry* **2004**, *43*, 7725–7735. [[CrossRef](#)]
38. Kobayashi, M.; Fujiwara, Y.; Goda, M.; Komeda, H.; Shimizu, S. Identification of active sites in amidase: Evolutionary relationship between amide bond- and peptide bond-cleaving enzymes. *Proc. Natl. Acad. Sci. USA* **1997**, *94*, 11986–11991. [[CrossRef](#)]
39. Mileni, M.; Garfunkle, J.; Ezzili, C.; Kimball, F.S.; Cravatt, B.F.; Stevens, R.C.; Boger, D.L. X-ray crystallographic analysis of alpha-ketoheterocycle inhibitors bound to a humanized variant of fatty acid amide hydrolase. *J. Med. Chem.* **2010**, *53*, 230–240. [[CrossRef](#)]
40. Tarzia, G.; Duranti, A.; Gatti, G.; Piersanti, G.; Tontini, A.; Rivara, S.; Lodola, A.; Plazzi, P.V.; Mor, M.; Kathuria, S.; et al. Synthesis and structure-activity relationships of FAAH inhibitors: Cyclohexylcarbamic acid biphenyl esters with chemical modulation at the proximal phenyl ring. *ChemMedChem* **2006**, *1*, 130–139. [[CrossRef](#)]
41. Otrubova, K.; Brown, M.; McCormick, M.S.; Han, G.W.; O’Neal, S.T.; Cravatt, B.F.; Stevens, R.C.; Lichtman, A.H.; Boger, D.L. Rational design of fatty acid amide hydrolase inhibitors that act by covalently bonding to two active site residues. *J. Am. Chem. Soc.* **2013**, *135*, 6289–6299. [[CrossRef](#)] [[PubMed](#)]
42. Gustin, D.J.; Ma, Z.; Min, X.; Li, Y.; Hedberg, C.; Guimaraes, C.; Porter, A.C.; Lindstrom, M.; Lester-Zeiner, D.; Xu, G.; et al. Identification of potent, noncovalent fatty acid amide hydrolase (FAAH) inhibitors. *Bioorg. Med. Chem. Lett.* **2011**, *21*, 2492–2496. [[CrossRef](#)] [[PubMed](#)]
43. Stewart, J.L.; McMahon, L.R. The fatty acid amide hydrolase inhibitor URB 597: Interactions with anandamide in rhesus monkeys. *Br. J. Pharmacol.* **2011**, *164*, 655–666. [[CrossRef](#)] [[PubMed](#)]



© 2019 by the authors. Licensee MDPI, Basel, Switzerland. This article is an open access article distributed under the terms and conditions of the Creative Commons Attribution (CC BY) license (<http://creativecommons.org/licenses/by/4.0/>).